Johann Radon Institute for
Computational and Applied Mathematics
Austrian Academy of Sciences (ÖAW)

Simulation results for a Finite Element based Cumulative Reconstructor

R. Wagner, A. Neubauer, R. Ramlau

RICAM-Report 2017-06

Simulation results for a Finite Element based Cumulative Reconstructor

Roland Wagner*, Andreas Neubauer†, Ronny Ramlau‡

March 16, 2017

Abstract

Modern ground-based telescopes rely on Adaptive Optics (AO) systems for the compensation of image degradation caused by atmospheric turbulences. Within an AO system, measurements of incoming light from guide stars are used to adjust deformable mirror(s) in real time that correct for atmospheric distortions. The incoming wavefront has to be derived from sensor measurements and this intermediate result is then translated into the shape(s) of the deformable mirror(s). Rapid changes of the atmosphere lead to the need of fast wavefront reconstruction algorithms.

In this paper, we review a fast matrix-free algorithm which was developed in [6] to reconstruct the incoming wavefront from Shack-Hartmann measurements based on a finite element discretization of the telescope aperture. The method is enhanced by a domain decomposition ansatz. We show that this new algorithm reaches the quality of standard approaches in end-to-end simulation while at the same time maintaining the speed of recently introduced solvers with linear order speed.

1 Introduction

The acquisition of high resolution images of astronomical objects requires requires ground-based extremely large telescopes (ELTs) with a primary mirror

*Johann Radon Institute for Computational and Applied Mathematics, Linz, Austria. roland.wagner@ricam.oeaw.ac.at

†Industrial Mathematics Institute, JKU Linz, Austria

‡Industrial Mathematics Institute, JKU Linz, Austria, and Johann Radon Institute for Computational and Applied Mathematics, Linz, Austria

of more than 30 m in diameter. A major drawback of ground-based telescopes is their decreased imaging quality due to turbulence in the atmosphere, which can be corrected by *Adaptive Optics (AO)* systems, see, e.g., [8].

In AO systems, measurements of incoming turbulent wavefronts from so-called guide stars are used to adjust a deformable mirror such that the incoming wavefront is corrected. Wavefront sensors (WFS) can only obtain indirect measurements, e.g., the Shack-Hartmann WFS measures the local gradient of a incoming wavefront. The available indirect measurements lead to the Inverse Problem of reconstructing a function from its averaged gradient. To tackle this problem, various methods have been developed in the past. Due to the large size of the resulting system for an ELT setting, a classical matrix-vector multiplication (MVM),i.e., the application of the (generalized) inverse of the matrix representing the sensor, is usually not fast enough to handle the reconstruction within the required time. Therefore, new methods as the Fractal Iterative Method (FrIM) [11] and the Cumulative Reconstructor with Domain decomposition (CuReD) (cf., [14, 9]) were developed, scaling both with $O(N)$, where N is the number of measurements from the WFS. These methods benefit from an iterative procedure with preconditioning and a matrix free algorithm, respectively, which both meet the speed requirements for ELTs, i.e., the incoming wavefront has to be reconstructed from the WFS measurements within 2 ms. Other fast methods were developed based on sparse matrices, making use of the Fourier transform or using iteratively a Tikhonov regularization (see, e.g., [3]) with different penalization terms (cf., e.g., [1, 4, 7, 12, 13, 2]).

In [6], a new algorithm was presented to reconstruct the incoming wavefront from Shack-Hartmann measurements in $O(N)$ operations. This algorithm is based on the same ideas as CuReD, but using a finite element basis to represent the wavefront. A treatment of rather general domains, including annular apertures, was already introduced there.

The goal of this paper is the evaluation of the reconstruction quality of this new cumulative reconstructor on finite element basis. Specifically, the task is to reconstruct the incoming wavefront from Shack-Hartmann measurements for a single conjugate adaptive optics (SCAO) system on a 42 m ELT.

Additonally, the algorithm is improved by introducing a domain decomposition ansatz. The results are compared to the existing results of CuReD and ESO's MVM in the ESO end-to-end simulation tool, Octopus.

The paper is structured as follows: In Section 2, we recall the algorithm.

In Section 3, we introduce two flavors of a domain decomposition ansatz and how the subdomains are connected in a proper way. In Section 4, we present the simulation results obtained in Octopus and compare them to the existing algorithms.

2 The finite element wavefront reconstruction algorithm revisted

In this section, we recall the wavefront reconstruction algorithm from [6]. Only the discretized version of the algorithm is presented, for a more detailed discussion we refer to the original work. As this algorithm works as cumulative reconstructor on a finite element basis, we call it FinECuRe.

A Shack-Hartmann WFS consists of a grid of small lenslets, called subapertures. In each of these subapertures, the average gradient of the incoming wavefront in two orthogonal directions is measured. From now on, we assume that the Shack-Hartmann WFS has $n \times n$ subapertures.

Let us denote the telescope aperture by Ω and decompose it into $N = n^2$ disjoint subapertures Ω_{ij}, $i, j \in \{1, \dots n\}$, fulfilling $\cup_{i,j}\Omega_{ij} = \Omega$. The Shack-Hartmann sensor operator $\Gamma = (\Gamma x, \Gamma y)$ is defined as

$$s_x[i,j] = (\Gamma_x \phi)[i,j] := \frac{1}{|\Omega_{ij}|} \int_{\Omega_{ij}} \phi_x(x,y)\, d(x,y),$$
$$s_y[i,j] = (\Gamma_y \phi)[i,j] := \frac{1}{|\Omega_{ij}|} \int_{\Omega_{ij}} \phi_y(x,y)\, d(x,y),$$

where $i, j \in \{1, \dots n\}$ and ϕ_x, ϕ_y denote the partial derivatives of ϕ. We define $s := (s_x, s_y) \in \mathbb{R}^N \times \mathbb{R}^N$. However, not all of these subapertures will be active in practice since the grid is square and the primary mirror of the telescope is usually only an annulus. Inactive subapertures will not return measurements and thus a wavefront reconstruction is not feasible on these parts, so let us from now on consider only active subapertures of the WFS. This situation is shown in Figure 1 for a general annular aperture.

The aim of the presented algorithm is to choose the approximate wavefront $\bar{\phi}$ such that the sensor measurements s are reproduced exactly, i.e.,

$$\Gamma\bar{\phi} = \Gamma R s = s,$$

where R is the reconstruction operator.

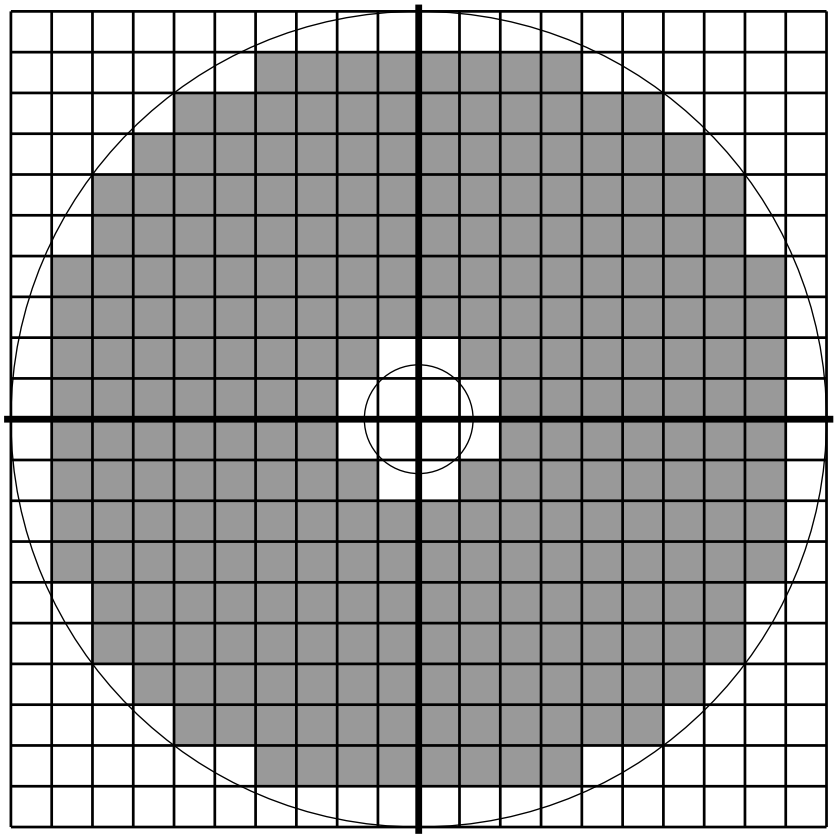

Figure 1: A general telescope aperture with the WFS subapertures. (from [6]).

We define the set of admissible indices as $\overline{\mathcal{M}}$, i.e., indices of the active subapertures, and define the reconstruction of the wavefront via a finite element representation as

$$Rs(x,y) = \bar{\phi}(x,y) = \sum_{(p,q)\in\overline{\mathcal{M}}} c_{p,q}\phi_{p,q}(x,y), \tag{1}$$

where the functions $\phi_{p,q}$ are piecewise linear functions satisfying

$$\phi_{p,q}(\bar{x}_{\tilde{p}}, \bar{y}_{\tilde{q}}) = \delta_{p,\tilde{p}}\delta_{q,\tilde{q}},$$

where $\delta_{r,t}$ denotes the usual Kronecker symbol. Due to this special choice, it holds that

$$\overline{\phi}(\bar{x}_p, \bar{y}_q) = c_{p,q}.$$

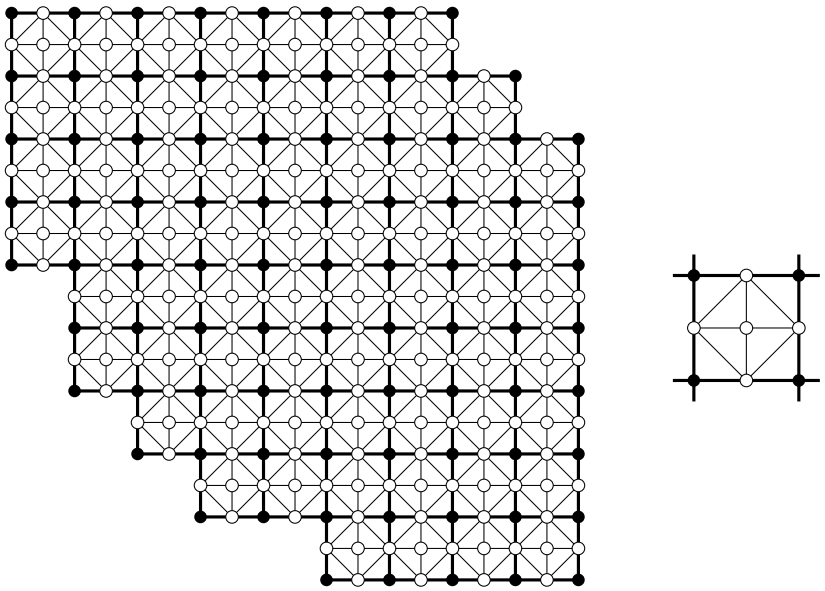

Figure 2: A part of a telescope aperture with WFS subapertures (bold lines). The dots indicate the nodes which are used for constructing the finite element reprensentation via piecewise linear functions (from [6]). Corners of subapertures of the WFS are filled dots, intermediate points are empty dots.

The underlying geometry can can be represented as a triangulation of Ω as shown in Figure 2.

As a Shack-Hartmann WFS cannot measure constant functions, known as piston mode, the algorithm should not introduce a constant shift to the reconstructed wavefront. Therefore, we assume that $\bar{\phi}$ should have mean zero, and it should furthermore be close to the exact solution ϕ. For the implementation, the formulae of [6, Section 3] have to be discretized. We need to compute sums over each line in x- and y-direction and shifts to connect the restored parts together. The corresponding formulae are recalled in Appendix A in (10)-(5). From there we get $l_x, l_y, w_{xx}, w_{yy}, w_{xy}, w_{yx}, g_y, g_x, \eta_y, \eta_x$, and can compute the following approximations of $\tilde{\varphi}$ as one-sided limits from all four possible directions, i.e., $\tilde{\phi}[i, j^+], \tilde{\phi}[i, j^-], \tilde{\phi}[i^+, j], \tilde{\phi}[i^-, j]$ for all admissible pairs (i, j), as follows

$$\tilde{\phi}[i, j-1^+] = l_x[i, j] - w_{xx}[j][\underline{p}_j, \overline{p}_j] + w_{yx}[j-1][\underline{p}_j, \overline{p}_j] + g_y[j] - \tilde{\eta}_y - \bar{\eta}_y, \tag{2}$$

$$\tilde{\phi}[i, j^-] = l_x[i, j] - w_{xx}[j][\underline{p}_j, \overline{p}_j] + w_{yx}[j][\underline{p}_j, \overline{p}_j] + g_y[j] - \tilde{\eta}_y - \bar{\eta}_y, \tag{3}$$

with $1 \le j \le N_y, \underline{p}_j \le i \le \overline{p}_j$, and,

$$\tilde{\phi}[i-1^+, j] = l_x[i,j] - w_{yy}[i][\underline{q}_i, \overline{q}_i] + w_{xy}[i-1][\underline{q}_i, \overline{q}_i] + g_x[i] - \tilde{\eta}_x - \bar{\eta}_x, \quad (4)$$

$$\tilde{\phi}[i^-, j] = l_x[i,j] - w_{yy}[i][\underline{q}_i, \overline{q}_i] + w_{xy}[i][\underline{q}_i, \overline{q}_i] + g_x[i] - \tilde{\eta}_x - \bar{\eta}_x, \quad (5)$$

with $1 \le i \le N_x, \underline{q}_i \le j \le \overline{q}_i$. The numbers $\underline{p}_j, \overline{p}_j$ and $\underline{q}_i, \overline{q}_i$, respectively, are fixed by the underlying geometry of the WFS, see [6, Section 2].

From these approximations we compute $\bar{\phi}$ at the corners of Ω_{ij} as

$$c_{2i,2j} = \frac{\tilde{\phi}[i,j^-]\mu(i,j) + \tilde{\phi}[i,j^+]\mu(i,j+1)}{2(\mu(i,j)+\mu(i,j+1))} + \frac{\tilde{\phi}]i^-,j]\nu(i,j) + \tilde{\phi}[i^+,j]\nu(i+1,j)}{2(\nu(i,j)+\nu(i+1,j)} \quad (6)$$

for all admissible values i, j and where

$$\mu(i,j) = \begin{cases} 2, & \underline{p}_j < i < \overline{p}_j, \\ 1, & i \in \{\underline{p}_j, \overline{p}_j\}, \\ 0, & else, \end{cases} \qquad \nu(i,j) = \begin{cases} 2, & \underline{q}_i < j < \overline{q}_i, \\ 1, & j \in \{\underline{q}_i, \overline{q}_i\}, \\ 0, & else. \end{cases}$$

Note that for boundary nodes, some values are not well-defined, but the appropriate weights are 0 anyways.

The values of $\bar{\phi}$ at intermediate points can be calculated by

$$c_{2i,2j-1} = \tilde{\phi}[i, j-1^+] + \tilde{\phi}[i,j^-] - \frac{1}{2}(c_{2i,2j-2} + c_{2i,2j}), \quad (7)$$

$$c_{2i-1,2j} = \tilde{\phi}[i-1^+, j] + \tilde{\phi}[i^-,j] - \frac{1}{2}(c_{2i-2,2j} + c_{2i,2j}), \quad (8)$$

$$c_{2i-1,2j-1} = \frac{1}{4}(\tilde{\phi}[i-1, j-1^+] + \tilde{\phi}[i,j^-] + \tilde{\phi}[i-1^+, j-1] + \tilde{\phi}[i^-,j]). \quad (9)$$

These steps are summarized in Algorithm 1.

We emphasize that the reconstruction algorithm is linear with using only $14N$ operations for the first four steps and the first three steps can be performed independently on each subdomain, if we have to split the domain for geometrical reasons. The last two steps require another $12N$ operations.

In the control system of a big telescope, the reconstructed wavefront has to be mapped into actuator commands for the deformable mirror. Depending on the actual geometry of the deformable mirror, it might be possible to omit the last two steps, e.g., if the actuators of the deformable mirror are perfectly aligned with the corners of the subapertures.

Algorithm 1 FinECuRe (from [6])

Let $s = (s_x, s_y) \in \mathbb{R}^N \times \mathbb{R}^N$. Then $Rs = \phi$ is defined as in (1). For the computation of the appropriate coefficients $c_{p,q}$ the following steps have to be performed:

(i) Calculate the chains l_x, l_y according to (10), (11), respectively.

(ii) Calculate $w_{xx}, w_{yx}, w_{yy}, w_{xy}$, the jump numbers f_x, f_y, the sums g_x, g_y, and the constants $\widetilde{\eta}_x, \widetilde{\eta}_y, \overline{\eta}_x, \overline{\eta}_y$ according to their definitions in (12) - (27).

(iii) Calculate the approximations $\tilde{\phi}(i, j^+), \tilde{\phi}(i, j^-), \tilde{\phi}(i^+, j), \tilde{\phi}(i^-, j)$ from (2) - (5).

(iv) Compute the corner nodes $c_{2i,2j}$, given by (6).

(v) Compute the intermediate nodes at the edges $c_{2i,2j-1}, c_{2i-1,2j}$, from (7) and (8).

(vi) Finally, compute the subaperture mid point nodes $c_{2i-1,2j-1}$, from (9).

(vii) Compute $\bar{\phi}$ from (1).

3 Domain decomposition

The annular shape of a telescope apertures causes problems in calculating the lines l_x, l_y which cross the aperture. Additionally, noise propagation by the reconstructor adds additional errors in the reconstruction. As the idea for reconstructing a wavefront from its gradient is based on simply integrating over lines of measurements across the aperture, noise in the measurements will add up and change the resulting wavefront. To overcome this problem, we want to restrict the area on which the reconstruction algorithm is applied. This reduces the length of the calculated chains and therefore the propagation of measurement noise. We start by decomposing the telescope apertures Ω into small subdomains Ω_i with the properties that they fully cover the apertures

$$\Omega = \bigcup_i \Omega_i,$$

and the intersection of two subdomains contains only the boundary:

$$\Omega_i \cap \Omega_j = \partial\Omega_i \cap \partial\Omega_j, \qquad \forall i \neq j.$$

For proper application of the algorithm, the splitting should be done such that each domain of a subapertures of the Shack-Hartmann WFS belongs only to one of the subdomains. In Figure 1, we present a simple way of splitting a telescope aperture into four subdomains. To obtain a full reconstructed wavefront, the parts on the different subdomains have to be connected again.

The splitting into subdomains and following connection to a reconstructed wavefront on the full telescope aperture can be done in many different ways. In the following, we present two different approaches that yield good results: the first one suggested in [6, Remark 3.2], and the second one presented in [10, Section 3]. As both of them include a domain decomposition to FinECuRe, we abbreviate this enhanced version as FinECuReD.

3.1 Exact connection

The first approach works straightforward, e.g., if Ω is symmetric with respect to the x- and y-axis and the origin of the coordinate system is the midpoint of the aperture, that it is split along these axis and that all four regions are of the same size (as in Figure 1). The main idea is to shift the reconstruction in the four subdomains accordingly to guarantee continuity and zero mean for the reconstructed wavefront over the whole aperture Ω [6].

For this approach, one has to substitute the constants $\eta_x = \tilde{\eta}_x + \bar{\eta}_x, \eta_y = \tilde{\eta}_y + \bar{\eta}_y$ by appropriate values in each of the subdomains. For simplicity, these constants are denoted $c^{ul}, c^{ur}, c^{ll}, c^{lr}$, where the superscripts stand for upper and lower in the first and left and right in the second letter. All other values are calculated only for the respective part of Ω.

The constants for substituting η_y were already presented in [6], so let us just recall their discretized versions for completeness. Note, that all indices are related not to the whole aperture, but only to the corresponding quarter.

$$\begin{aligned}
c_y^{ll} &= \frac{1}{4}(\eta_y^{ll} + \eta_y^{ul} + \eta_y^{lr} + \eta_y^{ur} + \kappa_{1,y} + \kappa_{2,y} + 2\kappa_{3,y}),\\
c_y^{ul} &= c_y^{ll} - \kappa_{1,y},\\
c_y^{lr} &= c_y^{ll} - \kappa_{3,y},\\
c_y^{ur} &= c_y^{lr} - \kappa_{2,y},\\
\kappa_{1,y} &= [w_{yx}[N_y][\underline{p}_{N_y}, \overline{p}_{N_y}] + g_y[N_y]]^{ll},\\
\kappa_{2,y} &= [w_{yx}[1][\underline{p}_1, \overline{p}_1] + g_y[N_y]]^{lr},\\
\kappa_{3,y} &= [l_x[N_x, 1] - w_{xx}[1][\underline{p}_1, \overline{p}_1] + w_{yx}[1][\underline{p}_1, \overline{p}_1] + g_y[1]]^{ll}\\
&\quad - [-w_{xx}[1][\underline{p}_1, \overline{p}_1] + w_{yx}[1][\underline{p}_1, \overline{p}_1] + g_y[1]]^{lr}.
\end{aligned}$$

For the connection in y-direction some adjustments of the constants are necessary and the correct constants are given by

$$\begin{aligned}
c_{ll} &= \frac{1}{4}(\eta_x^{ll} + \eta_x^{ul} + \eta_x^{ur} + \eta_x^{lr} + \kappa_{1,x} + \kappa_{2,x} + 2\kappa_{3,x}),\\
c_{ul} &= c_{ll} - \kappa_{3,x},\\
c_{ur} &= c_{ul} - \kappa_{1,x},\\
c_{lr} &= c_{ll} - \kappa_{2,x},\\
\kappa_{1,x} &= [w_{xy}[N_x][\underline{q}_{N_x}, \overline{q}_{N_x}] + g_x[N_x]]^{ul},\\
\kappa_{2,x} &= [w_{xy}[N_x][\underline{q}_{N_x}, \overline{q}_{N_x}] + g_x[N_x]]^{ll},\\
\kappa_{3,x} &= [l_y[1, N_y] - w_{yy}[1][\underline{q}_1, \overline{q}_1]]^{ll} + [w_{yy}[1][\underline{q}_1, \overline{q}_1]^{ul}.
\end{aligned}$$

3.2 Connection by averaging on the boundary

The following idea, originally presented in [10], is a hierarchical approach. We start as in Section 3.1 by splitting the aperture into four subdomains. This is called subdivision level 1. It is possible to make the subdomains even smaller, denoted as adding a new level of subdivision. When a new level of

subdivision is added, the existing subdomains are split into four parts. In Figure 3, the decomposition at the first level is shown by dashed lines and the second level is indicated by dotted lines in the upper-left subdomain. Therefore, the length of lines that have to be calculated is divided by two with each new level of decomposition. Thus we get a hierarchical decomposition of the telescope aperture.

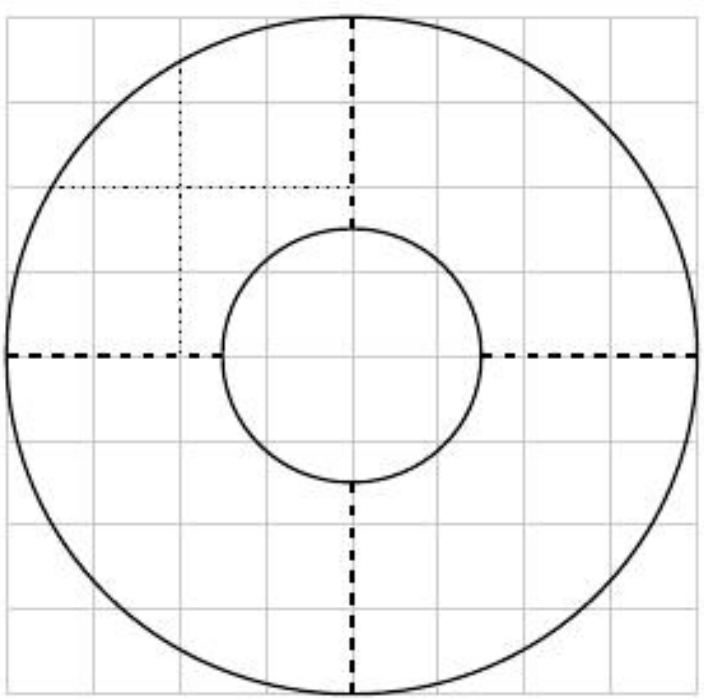

Figure 3: A possible decomposition of the domain Ω (from [10]).

For reconstructing the wavefront with this decomposition approach, our reconstruction algorithm is used on each subdomain separately. These subdomains are now much smaller as the full aperture and thus the effect of noise propagation is reduced and the reconstruction quality improves.

As the reconstructed wavefront has values at the boundaries, the mean value of a common boundary of two neighboring subdomains can be used to estimate the shift of the parts with respect to each other. For fitting together all parts, one has to start on the finest level and fit together always four parts.

To start, we have to compute the differences at a common boundary, i.e.,

$$d_{i,j} = \text{mean}(\varphi_i|_{\partial\Omega_i \cap \partial\Omega_j} - \varphi_j|_{\partial\Omega_i \cap \partial\Omega_j}),$$

for the pairs of subdomains $\{i, j\} = \{1, 2\}, \{1, 3\}, \{2, 4\}, \{3, 4\}$ on the finest level, with an appropriate numbering.

These differences are circularly connected and due to measurement noise this circle might be not rotation free. Hence, the error, calculated via

$$\epsilon = d_{1,2} + d_{2,4} - d_{1,3} - d_{3,4},$$

has to be distributed equally over all differences, i.e., add respectively subtract $(\epsilon/4)$ from d_i, j. The reconstruction φ_i can be left unshifted as the mean value of the global reconstruction is finally shifted to zero and there is no need to handle this locally. The other parts are then shifted as

$$\begin{aligned}
\tilde{\varphi}_2 &= \phi_2 + d_{1,2}, \\
\tilde{\varphi}_3 &= \phi_3 + d_{1,3}, \\
\tilde{\varphi}_4 &= \phi_4 + d_{1,2} + d_{2,4}.
\end{aligned}$$

The connection has to be done on each level, starting from the innermost. As a last step the reconnected wavefront has to be shifted to restore a zero mean value.

For FinECuReD, the connection of the subdomains requires a bit more effort than for the usual CuReD as all the shifts have to be performed before step (iv) of Algorithm 1 and the boundaries are not the same for the four approximations calculated in step (iii).

4 Results

4.1 Simulation results in Octopus

We incorporated a MATLAB implementation of the algorithm into the ESO end-to-end simulation tool Octopus [5] to test and verify the theoretical results. Benchmark results were available for ESO's MVM and CuReD. For all simulations, we used the setting in Table 1 and let the photon flux range from 1 to 10000 photons per subapertures per frame, and no read-out-noise was assumed. As comparison results were available for a telescope with 42 m diameter, we used this setting even though the current plans of the E-ELT

Table 1: **Description of the simulated SCAO system**

Telescope diameter	42 m
central obstruction	11.76 m
1 NGS Shack-Hartmann WFS	84×84 subapertures
wavelength λ	0.589 μm
WFS integration time	2 ms
1 DM at height 0 m	closed loop
DM actuator spacing	0.5 m

have a smaller diameter.

All tests are performed over 1000 timesteps, i.e., 2 seconds of real time. For the simulations, we use the ESO 9 layer standard atmosphere with $r_0 = 12.9\ cm$ at a wavelength of $500\mu m$. This setting represents median seeing conditions for Cerro Armazones, the site of the to be built E-ELT in the Atacama desert in Chile. In the AO control, we use a simple integrator where only the loop gain has to be adjusted when the flux of the guide star varies. We optimized the loop gain for different guide star flux.

The implementation of FinECuReD needs geometry preprocessing to get the values for $\underline{p}_j$, $\overline{p}_j$, $\underline{q}_i$ and $\overline{q}_i$ used for calculating the chains in both directions. This has to be done once for each subdomain, can be parallelized and can be done before the reconstruction starts.

As already mentioned in Section 2, the last two steps (v) and (vi) of the algorithm are omitted, as the actuators are located at the corners of the subapertures. For connecting the subdomains, both methods discussed in Section 3 have been implemented and tested. The second method was tested for $l = 1, 2, 4$ levels of subdivision, meaning 2^l subdomains in each direction. The splitting into more than 4 subdomains increases the quality significantly for low flux.

As a reference, we use results for these cases obtained with ESO-MVM tuned by Miska Le Louarn and CuReD using 4 levels of subdivision tuned by Matthias Rosensteiner.

In Figure 4, the simulation results are plotted. We compare our results for different subdivision levels (1,2,4) and for the exact connection method

from Section 3.1 to the references from ESO's MVM and CuReD. One can see that for high flux the new FinECuReD performs at same level as CuReD and MVM. In the low flux cases, similarly to the original CuReD also FinECuReD benefits from more levels of subdivision, and the results stay comparable to the references. Unfortunately, we do not get these good results using the exact connection method in the very low flux cases. This is also due to the high noise propagation when using only one level of subdivision. Note that the gain for FinECuReD can always be chosen in the same way as for CuReD.

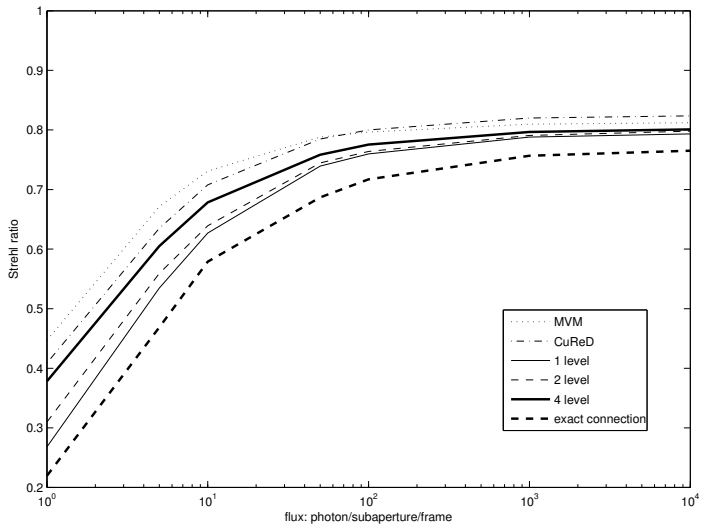

Figure 4: Simulation results for different levels of subdivision of FinECuReD. MVM (dotted) and CuReD (dash-dotted) are used as references. The results for 1, 2, 4 levels are calculated with averaging on the boundaries. Exact connection means that the connection method suggested in Section 3.1 was used.

4.2 Speed estimates

As CuReD and FinECuReD have the same computational complexity (cf, [6], and, [14], respectively), they should have approximately the same runtime, although this could not be tested due to the lack of an RTC implementation of FinECuReD.

In [10, Section 8] some tests for an RTC prototype of CuReD were computed. Since the computational complexity and the type of operations needed to run FinECuRed are the same, we expect a comparable runtime. There it was shown that CuReD can be easily run on a standard of-the-shelf hardware sufficiently fast to control an AO system with a 84×84 Shack-Hartmann WFS. In contrast to that an MVM run on the same four Intel hexacore processors on a speed of 2.66 GHz would take 18 ms. For a much larger system, e.g., a 200×200 Shack-Hartmann WFS, CuReD parallelized on 10 cores still only needs 270 μs, which is fast enough for a real AO system, whereas an MVM needs 510 ms on the same machine.

4.3 Noise propagation

As sensor measurements are always effected by noise, we want to present an estimate for the noise propagation through the reconstruction process in our algorithm. However, we can estimate how close our reconstruction is to exact incoming wavefront, as the result in [6, Section 5] gives a worst-case estimate on how noise and the approximation error from the reconstruction algorithm affect the reconstructed wavefront.

Usually, instead of exact data $s = \Gamma\varphi$, only noisy measurements $s^\delta = \Gamma\varphi + \delta s$ are available. We assume that $|\delta s_x[i,j]| \leq \delta$ and $|\delta s_y[i,j]| \leq \delta$ for some $\delta \geq 0$. Based on [1], φ may be expected to be smooth enough for all conditions in the estimates in [6] to hold. For a 84×84 Shack-Hartmann WFS as in our simulated system, this leads to the following error estimate on each quarter of Ω, denoted by Ω_i:

$$\|\varphi - Rs^\delta\|_\infty \leq 11.25 \cdot L_{5/6} + 664.65 \cdot \delta,$$

where $L_{5/6}$ is the Hölder constant of the corresponding function space. The first part depends non-linearly on the subaperture size h, and the shape of Ω_i, the second part depends on the shape of Ω_i and linearly on the width of Ω_i. This clearly shows that splitting Ω into smaller parts as only into quarters will improve the reconstruction quality as it decreases noise propagation.

Additionally, similarly to [10], we compute the noise propagation under the assumption of white noise (i.e., Gaussian, independent, and uniform on all subapertures) as

$$mse = \frac{\operatorname{trace}(MM^T)}{N},$$

where M is the matrix representation of FinECuReD, *trace* is the sum of the elements along the main diagonal of a matrix, and N is the number of subapertures. Note that M looks different for the different approaches from Section 3. For the original version, presented in Section 3.1, the propagation of noise is rather high, with $mse = 44.6$. When using the hierarchical domain decomposition approach, the propagation of noise can be bounded to $mse = 3.44$ for four levels of subdivision, $mse = 4.7$ for two levels of subdivision, and $mse = 6.2$ for one level of subdivision.

5 Conclusion

In this paper, we demonstrated that the new algorithm FinECuReD performs stable with respect to different photon flux and comparable in terms of quality to the existing MVM and CuReD. We showed that by using a domain decomposition ansatz, we can overcome problems with noise and error propagation. Compared to the original CuReD, we use approximately the same loop gain in our tests, so unfortunately we cannot improve the existing algorithms in this point. However, in terms of speed our algorithm clearly outperforms an MVM and the only parameter to be adjusted is the loop gain. All together, FinECuReD offers a good alternative to existing algorithms for wavefront reconstruction on ELTs.

Acknowledgments

We want to thank Miska Le Louarn and Matthias Rosensteiner for providing the results from ESO's MVM and CuReD, respectively. This work was funded by the Austrian Ministry of Research (Hochschulraumstrukturmittel).

References

[1] B.L. Ellerbroek. Efficient computation of minimum-variance wavefront reconstructors with sparse matrix techniques. *J. Opt. Soc. Am.*, 19(9):1803–1816, 2002.

[2] B.L. Ellerbroek and C.R. Vogel. Inverse problems in astronomical adaptive optics. *Inverse Problems*, 25(6):063001, 2009.

[3] H.W. Engl, M. Hanke, and A. Neubauer. *Regularization of Inverse Problems*. Kluwer Academic Publishers, Dordrecht, Boston, London, 2000.

[4] L. Gilles, C.R. Vogel, and B.L. Ellebroek. Multigrid preconditioned conjugate-gradient method for large-scale wave-front reconstruction. *J. Opt. Soc. Am. A*, 19(6):1817–1822, 2002.

[5] Miska Le Louarn, Christophe Verinaud, Visa Korkiakoski, Norbert Hubin, and Enrico Marchetti. Adaptive optics simulations for the European Extremely Large Telescope - art. no. 627234. In *Advances in Adaptive Optics II, Prs 1-3*, volume 6272, pages U1048–U1056, 2006.

[6] A. Neubauer. A new cumulative wavefront reconstructor for the Shack-Hartmann sensor. *J. Inv. Ill-Posed Problems*, 21:451–476, 2013.

[7] L.A. Poyneer, D.T. Gavel, and J.M. Brase. Fast wave-front reconstruction in large adaptive optics systems with use of the Fourier transform. *J. Opt. Soc. Am. A*, 19(10):2100–2111, 2002.

[8] F. Roddier. *Adaptive Optics in Astronomy.* Cambridge, U.K. ; New York : Cambridge University Press, Cambridge, 1999.

[9] M. Rosensteiner. Cumulative reconstructor: fast wavefront reconstruction algorithm for Extremely Large Telescopes. *J. Opt. Soc. Am. A*, 28(10):2132–2138, Oct 2011.

[10] M. Rosensteiner. Wavefront reconstruction for extremely large telescopes via CuRe with domain decomposition. *J. Opt. Soc. Am. A*, 29(11):2328–2336, Nov 2012.

[11] Michel Tallon, Clémentine Béchet, Isabelle Tallon-Bosc, Miska Le Louarn, E Thiébaut, Richard Clare, and Enrico Marchetti. Performances of MCAO on the E-ELT using the fractal iterative method for fast atmospheric tomography. *Adaptive Optics for ELTs II*, 2011.

[12] E. Thiébaut and M. Tallon. Fast minimum variance wavefront reconstruction for extremely large telescopes. *J. Opt. Soc. Am. A*, 27:1046–1059, 2010.

[13] C.R. Vogel and Q. Yang. Multigrid algorithm for least-squares wavefront reconstruction. *Applied Optics*, 45(4):705–715, 2006.

[14] M. Zhariy, A. Neubauer, M. Rosensteiner, and R. Ramlau. Cumulative wavefront reconstructor for the Shack-Hartman sensor. *Inverse Problems and Imaging*, 5(4):893–913, Nov 2011.

A Recalling all quantities for Algorithm 1

We recall the discretized versions of all needed quantities from [6]. For $1 \leq j \leq N_y$, $1 \leq i \leq N_x$, $1 \leq i_1 < i_2 \leq N_x$, $1 \leq j_1 < j_2 \leq N_y$, $h > 0$, the subaperture size in meter, and $s_x[i,j]$ and $s_y[i,j]$ the WFS measurements at subaperture $[i,j]$, we have

$$l_x[i,j] = h \sum_{p=\underline{p}_j+1}^{i} s_x[p,j], \tag{10}$$

$$l_y[i,j] = h \sum_{q=\underline{q}_i+1}^{j} s_y[i,q], \tag{11}$$

$$\tilde{w}_{xx}[j][i_1,i_2] = \frac{1}{2} \sum_{p=i_1+1}^{i_2} (l_x[p-1,j] + l_x[p,j]), \tag{12}$$

$$w_{xx}[j][i_1,i_2] = (i_2 - i_1)^{-1} \tilde{w}_{xx}[j][i_1,i_2], \tag{13}$$

$$\tilde{w}_{yx}[j][i_1,i_2] = \sum_{p=i_1+1}^{i_2} l_y[p,j], \tag{14}$$

$$w_{yx}[j][i_1,i_2] = (i_2 - i_1)^{-1} \tilde{w}_{yx}[j][i_1,i_2], \tag{15}$$

$$\tilde{w}_{yy}[i][j_1,j_2] = \frac{1}{2} \sum_{q=j_1+1}^{j_2} (l_y[i,q-1] + l_y[i,q]), \tag{16}$$

$$w_{yy}[i][j_1,j_2] = (j_2 - j_1)^{-1} \tilde{w}_{yy}[i][j_1,j_2], \tag{17}$$

$$\tilde{w}_{xy}[i][j_1,j_2] = \sum_{q=j_1+1}^{j_2} l_x[i,q], \tag{18}$$

$$w_{xy}[i][j_1,j_2] = (j_2 - j_1)^{-1} \tilde{w}_{xy}[i][j_1,j_2]. \tag{19}$$

For $1 \le n \le k$, define:

$$\begin{aligned} f_y[n] &= (w_{yx}[\sigma_n][\underline{p}_{\sigma_n}, \overline{p}_{\sigma_n}] - w_{yx}[\sigma_n][\underline{p}_{\sigma_n+1}, \overline{p}_{\sigma_n+1}]) \\ &\quad + (w_{xx}[\sigma_n+1][\underline{p}_{\sigma_n+1}, \overline{p}_{\sigma_n+1}] - w_{xx}[\sigma_n+1][\alpha_n, \beta_n]) \\ &\quad + (w_{xx}[\sigma_n][\alpha_n, \beta_n] - w_{xx}[\sigma_n][\underline{p}_{\sigma_n}, \overline{p}_{\sigma_n}], \\ \alpha_n &= \max\{\underline{p}_{\sigma_n}, \underline{p}_{\sigma_n+1}\}, \\ \beta_n &= \min\{\underline{p}_{\sigma_n}, \underline{p}_{\sigma_n+1}\}, \end{aligned} \tag{20}$$

$$g_y[j] = \sum_{\substack{n=1 \\ \sigma_n < j}}^{k-1} f_y[n], \qquad 1 \le j \le N_y, \tag{21}$$

$$\tilde{\eta}_y = N^{-1} \sum_{n=2}^{k} g_y[\sigma_n](\overline{p}_{\sigma_n} - \underline{p}_{\sigma_n})(\sigma_n - \sigma_{n-1}), \tag{22}$$

$$\bar{\eta}_y = N^{-1} \sum_{i=1}^{N_x} \tilde{w}_{yy}[i][\underline{q}_i, \overline{q}_i]. \tag{23}$$

Analogously, we define for $1 \le n \le l$,

$$\begin{aligned} f_x[n] &= (w_{xy}[\tau_n][\underline{q}_{\tau_n}, \overline{q}_{\tau_n}] - w_{xy}[\tau_n][\underline{q}_{\tau_n+1}, \overline{q}_{\tau_n+1}]) \\ &\quad + (w_{yy}[\tau_n+1][\underline{q}_{\tau_n+1}, \overline{q}_{\tau_n+1}] - w_{yy}[\tau_n+1][\gamma_n, \delta_n]) \\ &\quad + (w_{yy}[\tau_n][\gamma_n, \delta_n] - w_{yy}[\tau_n][\underline{q}_{\tau_n}, \overline{q}_{\tau_n}], \\ \gamma_n &= \max\{\underline{q}_{\tau_n}, \underline{q}_{\tau_n+1}\}, \\ \delta_n &= \min\{\underline{q}_{\tau_n}, \underline{q}_{\tau_n+1}\}, \end{aligned} \tag{24}$$

$$g_x[i] = \sum_{\substack{n=1 \\ \tau_n < i}}^{l-1} f_x[n], \qquad 1 \le i \le N_x, \tag{25}$$

$$\tilde{\eta}_x = N^{-1} \sum_{n=2}^{l} g_x[\sigma_n](\overline{q}_{\tau_n} - \underline{q}_{\tau_n})(\tau_n - \tau_{n-1}), \tag{26}$$

$$\bar{\eta}_x = N^{-1} \sum_{i=1}^{N_y} \tilde{w}_{yy}[j][\underline{p}_j, \overline{p}_j]. \tag{27}$$